

The Control of Self-Propelled Microjets Inside a Microchannel With Time-Varying Flow Rates

Islam S. M. Khalil, *Member, IEEE*, Veronika Magdanz, Samuel Sanchez, Oliver G. Schmidt, and Sarthak Misra, *Member, IEEE*

Abstract—We demonstrate the closed-loop motion control of self-propelled microjets inside a fluidic microchannel. The motion control of the microjets is achieved in hydrogen peroxide solution with time-varying flow rates, under the influence of the controlled magnetic fields and the self-propulsion force. Magnetic dipole moment of the microjets is characterized using the *U-turn* and the *rotating field* techniques. The characterized magnetic dipole moment has an average of 1.4×10^{-13} A.m² at magnetic field, linear velocity, and boundary frequency of 2 mT, 100 μ m/s, and 25 rad/s, respectively. We implement a closed-loop control system that is based on the characterized magnetic dipole moment of the microjets. This closed-loop control system positions the microjets by directing the magnetic field lines toward the reference position. Experiments are done using a magnetic system and a fluidic microchannel with a width of 500 μ m. In the absence of a fluid flow, our control system positions the microjets at an average velocity and within an average region-of-convergence (ROC) of 119 μ m/s and 390 μ m, respectively. As a representative case, we observe that our control system positions the microjets at an average velocity and within an average ROC of 90 μ m/s and 600 μ m and 120 μ m/s and 600 μ m when a flow rate of 2.5 μ l/min is applied against and along the direction of the microjets, respectively. Furthermore, the average velocity and ROC are determined throughout the flow range (0 to 7.5 μ l/min) to characterize the motion of the microjets inside the microchannel.

Index Terms—Magnetic torque, microchannel, microjets, micro-robots, motion control, self-propulsion, time-varying flow.

Manuscript received August 9, 2013; accepted September 3, 2013. This paper was recommended for publication by Associate Editor A. Ferreira and Editor B. J. Nelson upon evaluation of the reviewers' comments. This work was supported by funds from MIRA-Institute for Biomedical Technology and Technical Medicine, University of Twente, The Netherlands. The research leading to these results has also received funding from the Volkswagen Foundation (# 86 362) and the European Research Council under the European Union's Seventh Framework Programme (FP7/2007-2013)/ERC Grant 311529.

I. S. M. Khalil was with MIRA-Institute for Biomedical Technology and Technical Medicine, University of Twente, 7500 AE Enschede, The Netherlands. He is now with the German University in Cairo, New Cairo City 13411, Egypt (e-mail: islam.shoukry@guc.edu.eg).

V. Magdanz is with Institute for Integrative Nanosciences, IFW Dresden, 01069 Dresden, Germany (e-mail: v.magdanz@ifw-dresden.de).

S. Sanchez was with the Institute for Integrative Nanosciences, IFW Dresden, D-01069 Dresden, Germany. He is now with the Max Planck Institute for Intelligent Systems, 70569 Stuttgart, Germany (e-mail: Sanchez@is.mpg.de).

O. G. Schmidt is with the Institute for Integrative Nanosciences, IFW Dresden, 01069 Dresden, Germany, and also with the Material Systems for Nanoelectronics, University of Technology Chemnitz, 09107 Chemnitz, Germany (e-mail: o.schmidt@ifw-dresden.de).

S. Misra is with MIRA-Institute for Biomedical Technology and Technical Medicine, University of Twente, 7500 AE Enschede, The Netherlands (e-mail: s.misra@utwente.nl).

Color versions of one or more of the figures in this paper are available online at <http://ieeexplore.ieee.org>.

Digital Object Identifier 10.1109/TRO.2013.2281557

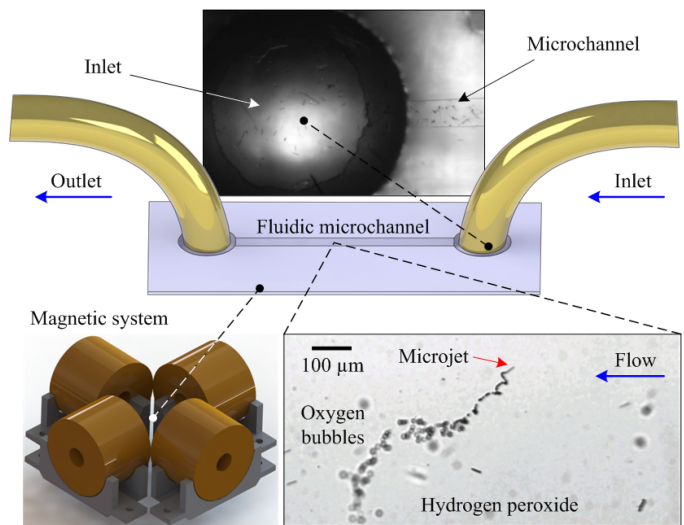


Fig. 1. Motion control of self-propelled microjets [12] inside a fluidic microchannel in the presence of time-varying flow rates. The microchannel has width and depth of 500 and 300 μ m, respectively. Microjets access the channel through one inlet of the microchannel and exit from another outlet. The flow rate of the hydrogen peroxide solution is controlled using a syringe pump (CMA 402 Syringe Pump, CMA Microdialysis, Kista, Sweden). The syringe pump (not shown) is connected to the inlet of the microchannel using a tube with inner diameter of 0.12 mm. The microjet is indicated using the red arrow and moves by the catalytic decomposition of the hydrogen peroxide solution. The microchannel is mounted in the center of an array of electromagnets to control the direction of the microjets under the influence of the controlled magnetic fields.

I. INTRODUCTION

THE implementation of magnetic-based targeted drug delivery systems using microrobots depends on *at least* three aspects. First, the ability of these systems to provide enough propulsion force to hold the microrobots against time-varying flow rates [1], [2]. Second, the availability of a real-time clinical imaging modality to provide motion control systems with the position of the microrobots [3]. Third, the robustness of the magnetic-based control system to parameter deviations, such as time-varying fluid viscosity and channel wall effect. These aspects can be investigated by controlling and analyzing the motion of a microrobot inside a controlled environment, such as a fluidic microchannel (see Fig. 1). This microchannel, along with a syringe pump, allow us to induce controlled flow rates and change the fluid viscosity to study the effect of the first and third aspects on the motion of microrobots. The motion of these microrobots is generated by pulling with the magnetic field gradients [4]–[10], inducing rotating magnetic fields [2], [11], or by the conversion of chemical energy to kinetic energy to provide

self-propulsion force [12], [13]. Microrobots that are propelled by pulling with the magnetic forces suffer from the limited projection distance of the field gradients, whereas self-propelled microrobots (microjets and magnetotactic bacteria) benefit from the larger projection distance of the magnetic fields. These fields only orient the microrobot along a desired direction. The self-propulsion force then provides translational motion along the field lines.

Sanchez *et al.* demonstrated that self-propelled microjets provide enough force to move against flowing streams of fluidic microchannels using open-loop control [12]. Furthermore, it has been demonstrated that microjets can transport spherical microparticles to a desired location. It has also been shown that self-propelled microjets can selectively transport large amounts of particles on the chip and murine CATH.a-differentiated cells by controlling the magnetic fields [14], [15]. Although this control allows us to achieve several nontrivial tasks, closed-loop control of microjets against and along the flowing streams of the fluid has not yet been shown. Nacev *et al.* demonstrated the localization of ferromagnetic nanoparticles inside rats (the slowest blood flow rates is approximately 0.1 mm/s) using external magnetic fields [16]. However, this control strategy is based on pulling the nanoparticles toward the desired position using external magnetic fields without measuring the location of the nanoparticles. Kummer *et al.* developed and utilized a five-degree-of-freedom magnetic system to puncture a blood vessel of a chorioallantoic membrane of a chicken embryo using a magnetic agent (two cubes with edge length of 800 μm) with permanent magnetization [4]. This drug delivery was done using relatively large field gradients, and in the absence of fluid flow.

In this study, we achieve the following:

- 1) modeling and characterization of microjets using the *U-turn* and *rotating field* techniques that are based on their motion analysis;
- 2) development of an experimental setup that allows us to induce controlled flowing streams against and along the motion of microjets;
- 3) closed-loop motion control of microjets inside a stationary hydrogen peroxide solution;
- 4) closed-loop motion control of microjets inside fluidic microchannels against and along the flowing streams of hydrogen peroxide solutions.

We study the closed-loop motion characteristics of a potential magnetic drug carrier, i.e., self-propelled microjet, in the presence and absence of controlled time-varying fluid flows. First, we characterize the magnetic properties of the microjets. This characterization includes the determination of the boundary frequency and magnetic dipole moment of the microjet. We utilize the *U-turn* [17], [18] and the *rotating field* [19] techniques to determine the average magnetic dipole moment of the microjets. Second, the characterized magnetic dipole moment is used in the realization of the magnetic force-current map of our magnetic system, shown in Fig. 2. This mapping is used in the implementation of a closed-loop control system that allows us to control the direction of the magnetic fields toward a reference position. Our system is used to achieve closed-loop point-to-point motion

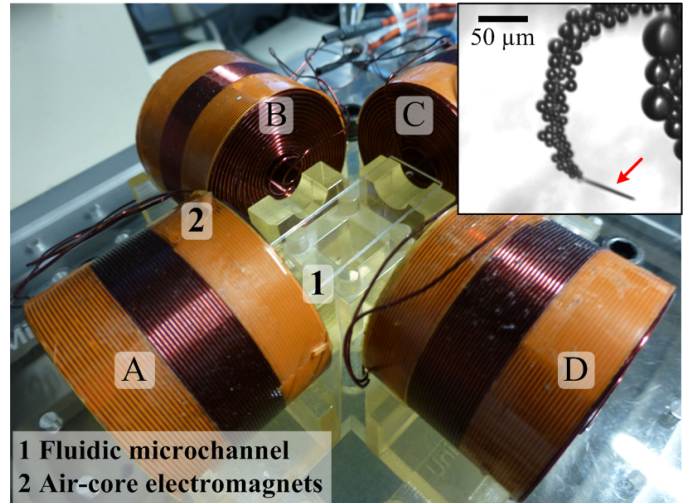


Fig. 2. Magnetic system for the wireless magnetic-based control of self-propelled microjets inside a fluidic microchannel. Motion of the microjets is controlled using the external magnetic fields that are generated by the electromagnets. Microjets move along the magnetic field lines using the propulsion force that is generated due to the ejecting oxygen bubbles from one of their ends, as shown in the inset. The red arrow indicates the microjet. The flow rates of the fluid (hydrogen peroxide solution) inside the microchannel are varied and controlled using a syringe pump (CMA 402 Syringe Pump, CMA Microdialysis, Kista, Sweden). Closed-loop motion characteristics at four flow rates (0, 2.5, 5, and 7.5 $\mu\text{l}/\text{min}$) are studied by the determination of the average velocity and positioning accuracy of microjets. The letters A, B, C, and D indicate the electromagnets. The system generates maximum magnetic field and magnetic field gradient of 15 mT and 60 mT/m, respectively.

control of microjets inside a fluidic microchannel. This motion control is implemented against and along the controlled fluid flow inside the microchannel at flow rates ranging from 0 to 7.5 $\mu\text{l}/\text{min}$. This range of flow rate is selected based on the blood flow rates of the veins, venule, and capillary of humans to assist future *in vivo* experiments [2].

The remainder of this paper is organized as follows. Section II provides a dynamical model of the self-propelled microjets in a fluid with time-varying flow. Furthermore, the characterization of the magnetic dipole moment is done using the *U-turn* and *rotating field* techniques. Section III presents the magnetic force-current map of our magnetic system and the design of a closed-loop control system. Moreover, finite-element (FE) simulation of the magnetic field lines and the magnetic force lines is presented along with a characterization of the frequency response of an air-core electromagnet of our magnetic system. The experimental results of the microjets in the absence and presence of time-varying flow rates (against and along the direction of motion of the microjets) are presented in Section IV. Finally, Section V concludes and provides directions for future work.

II. MODELING AND CHARACTERIZATION

Self-propelled microjets are made from rolled-up titanium, iron, and platinum layers [15]. These microjets are immersed in hydrogen peroxide solution with concentration that ranges from 5% to 15% to which small amounts of isopropanol and Triton X are added. Microjets orient along the magnetic field lines

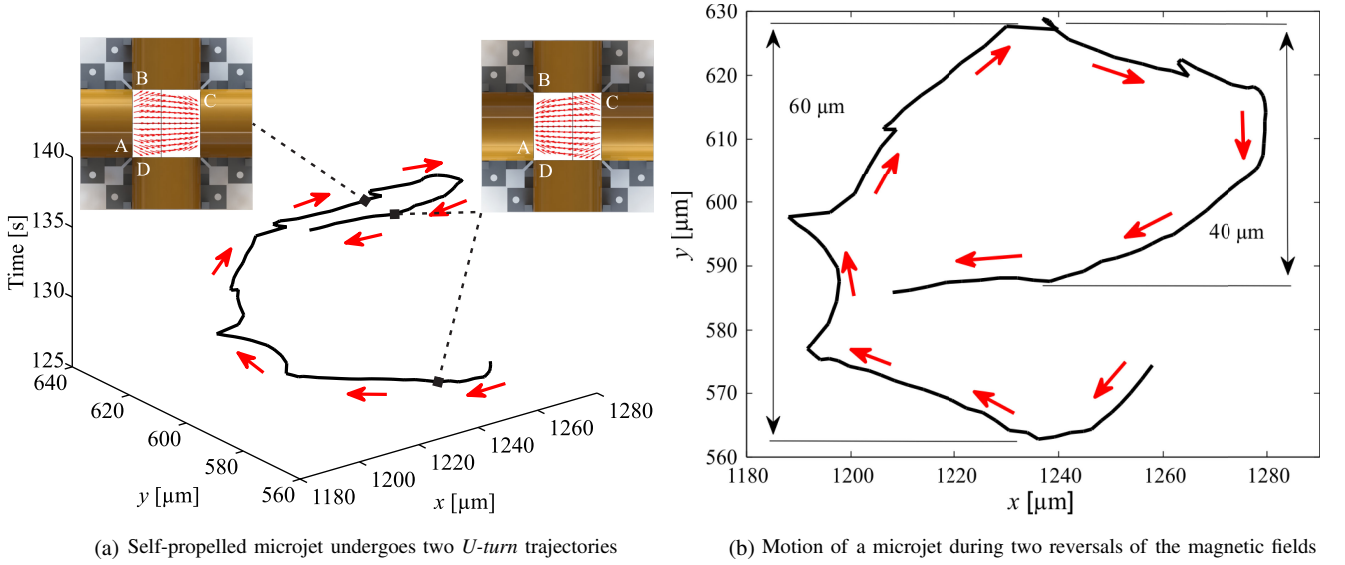


Fig. 3. Characterization of the magnetic dipole moment of the self-propelled microjets using the *U-turn* technique [17]. This characterization experiment is done inside a petri dish with hydrogen peroxide solution. (a) Microjet undergoes *U-turn* trajectories when the magnetic field is reversed. Average diameter of the *U-turn* trajectory is used to determine the magnetic dipole moment of the microjets. The insets show the electromagnets used to provide uniform magnetic field and field reversal in this characterization experiment. The magnetic field lines provided in the insets are generated using a FE model of our magnetic system. (b) Diameters of the *U-turn* trajectories, in this representative experiment, are 60 and 40 μm . The average *U-turn* diameter is 90 μm , and average magnetic dipole moment is calculated to be 1.3×10^{-13} A.m² using (7). The average is calculated from ten different *U-turn* experiments. Magnetic dipole moment is calculated using (7) and (8). The length and diameter of the microjet are 50 μm and 5 μm , respectively. The dynamic viscosity of the hydrogen peroxide solution is 1 mPa.s. The result of this characterization experiments is used in the realization of the magnetic force-current map (12).

using the magnetic torque exerted on their magnetic layers. The motion of the microjets along the field lines is achieved using the propulsion force of the ejecting oxygen bubbles due the catalytic decomposition of the hydrogen peroxide solution by the platinum layer of the microjet [20]. In this section, we model the motion of the microjets and characterize their magnetic dipole moment based on their motion analysis.

A. Modeling of Self-Propelled Microjets

In a low Reynolds number environment with a time-varying flow, motion of a self-propelled microjet is governed by the external magnetic fields and the self-propulsion force. The equation of motion of a microjet is given by

$$\mathbf{F}(\mathbf{P}) + \mathbf{f}(\mathbf{P}, t) + \rho_f \frac{D\mathbf{u}(\mathbf{P}, t)}{Dt} + \mathbf{F}_d(\dot{\mathbf{P}}) = 0 \quad (1)$$

where $\mathbf{F}(\mathbf{P}) \in \mathbb{R}^{3 \times 1}$ is the magnetic force at point ($\mathbf{P} \in \mathbb{R}^{3 \times 1}$), and $\mathbf{f}(\mathbf{P}, t) \in \mathbb{R}^{3 \times 1}$ is the self-propulsion force that is generated by the ejecting oxygen bubbles from one end of the microjet. Furthermore, $\mathbf{u}(\mathbf{P}, t)$ is the velocity field of a fluid of density (ρ_f). Furthermore, $\mathbf{F}_d(\dot{\mathbf{P}}) \in \mathbb{R}^{3 \times 1}$ denotes the drag force on the microjet. The substantial derivative ($\frac{D}{Dt}$) of the velocity field ($\mathbf{u}(\mathbf{P}, t)$) is given by

$$\frac{D\mathbf{u}(\mathbf{P}, t)}{Dt} = \frac{\partial \mathbf{u}(\mathbf{P}, t)}{\partial t} + \mathbf{u}(\mathbf{P}, t) \cdot \nabla \mathbf{u}(\mathbf{P}, t). \quad (2)$$

The magnetic force is given by

$$\mathbf{F}(\mathbf{P}) = (\mathbf{m} \cdot \nabla) \mathbf{B}(\mathbf{P}) \quad (3)$$

where $\mathbf{m} \in \mathbb{R}^{3 \times 1}$ and $\mathbf{B}(\mathbf{P}) \in \mathbb{R}^{3 \times 1}$ are the magnetic dipole moment of the microjet and the induced magnetic field, respec-

tively [21], [22]. A microjet also experiences magnetic torque given by

$$\mathbf{T}(\mathbf{P}) = \mathbf{m} \times \mathbf{B}(\mathbf{P}). \quad (4)$$

The self-propulsion force in (1) depends on the frequency of the ejecting oxygen bubbles. Therefore, it can be represented by the following periodic function:

$$\mathbf{f}(\mathbf{P}, t) = \mathbf{f}(\mathbf{P}, t + \tau) \quad (5)$$

where τ is the elapsed-time of the ejecting oxygen bubbles. Finally, the drag force in (1) is given by

$$\mathbf{F}_d(\dot{\mathbf{P}}) = \alpha \eta \dot{\mathbf{P}} \quad (6)$$

where α and η are the shape factor of the microjet and the dynamic viscosity of the fluid, respectively.

B. Characterization of the Magnetic Dipole Moment

Self-propelled microjets undergo *U-turn* and circular trajectories, when magnetic field reversals are initiated and rotating magnetic fields are applied, respectively. The diameter of the *U-turn* trajectory and the boundary frequency of the rotating microjets are used to determine their average magnetic dipole moment [23].

1) *U-Turn Technique*: Microjets use the magnetic torque to align along the field lines. Once the magnetic field is reversed, microjets undergo *U-turn* trajectories, as shown in Fig. 3(a). The frequency response of the electromagnets only influences the initiation time of the field reversal, as a low magnitude of torque will ultimately align the microjet along the field lines. The magnitude of the magnetic fields that is generated using our magnetic system is attenuated by 50% at a frequency of

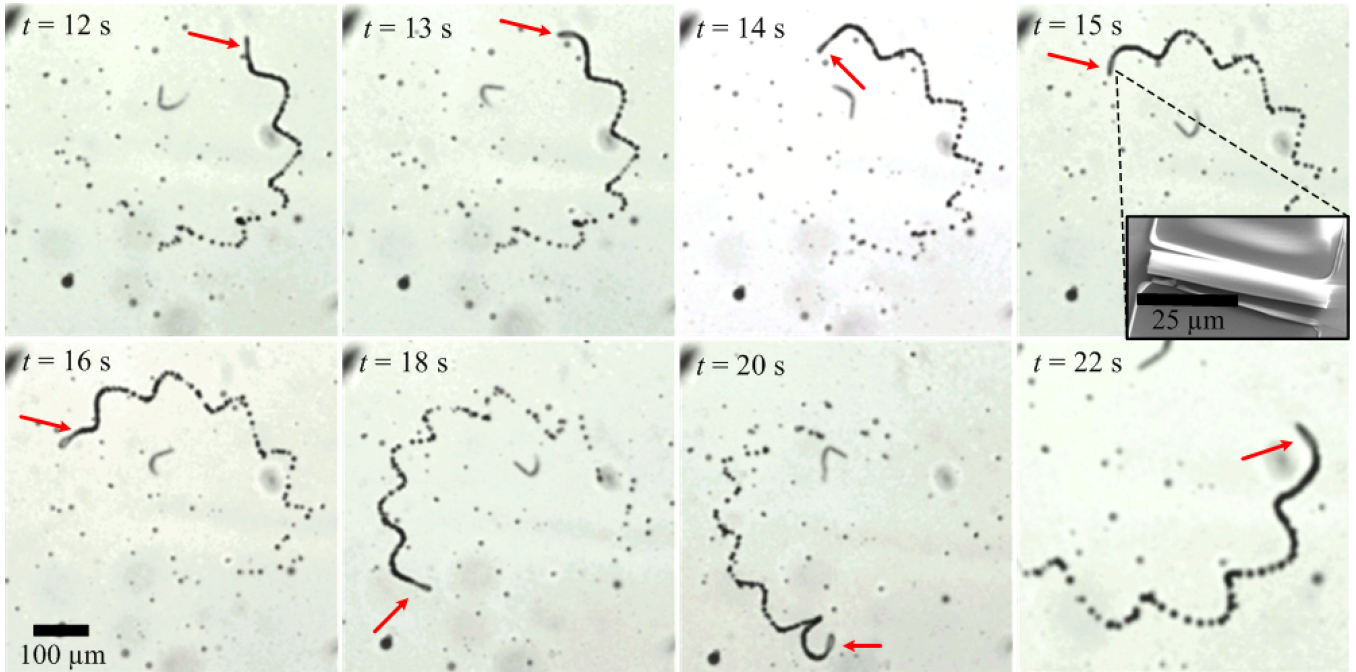


Fig. 4. Characterization of the magnetic dipole moment of the self-propelled microjets using the *rotating field* technique [19]. This characterization experiment is done inside a petri dish with hydrogen peroxide solution. Rotating magnetic fields are applied, and the frequency is gradually increased to determine the boundary frequency. In this representative experiment, the boundary frequency is 17 rad/s at magnetic field of 2 mT. The average boundary frequency is calculated from ten trials. The average boundary frequency is 25 rad/s, and the corresponding average magnetic dipole moment is 1.5×10^{-13} A.m², at magnetic field of 2 mT. The magnetic dipole moment is calculated using (8) and (9). The red arrows indicate the microjet, whereas the air bubbles represent the trajectory taken by the microjet. The inset shows a scanning electron microscopy image of a microjet fixed to its substrate.

100 Hz for a sinusoidal current input. The frequency response of an air-core electromagnet is characterized in Section III. In the representative experiment shown in Fig. 3, we initiate two magnetic field reversals, and the microjet undergoes two *U-turn* trajectories with diameters of 60 and 40 μm [see Fig. 3(b)]. The diameter (D) of the *U-turn* trajectory is given by [17]

$$D = \frac{\alpha\pi |\dot{\mathbf{P}}|}{|\mathbf{m}||\mathbf{B}(\mathbf{P})|} \quad (7)$$

where α is the rotational drag coefficient and is given by [24]

$$\alpha = \frac{\pi\eta L^3}{3} \left[\ln\left(\frac{L}{d}\right) + 0.92\left(\frac{d}{L}\right) - 0.662 \right]^{-1}. \quad (8)$$

In (8), η , L , and d are the dynamic viscosity of the hydrogen peroxide solution, length, and diameter of the microjet, respectively. We assume that the hydrogen peroxide solution has similar dynamic viscosity as water. The solution also contains 5% of Triton X and its effect on the dynamic viscosity is assumed negligible. We further assume that our microjets have cylindrical geometry in the calculation of α using (8). The *U-turn* characterization experiment is done ten times, and we observe that the average *U-turn* diameter is 90 ± 53 μm . The corresponding average magnetic dipole moment using (7) is 1.3×10^{-13} A.m² at the magnetic field and linear velocity of 2 mT and 100 $\mu\text{m/s}$, respectively. Our best hypothesis for the large variation in the diameter of the *U-turn* trajectory is the nonuniformity of the dynamic viscosity of the hydrogen peroxide and the bubbles–microjets interactions. First, the nonuniformity is due to the chemical reactions that locally occur at each microjet. Second,

interaction forces between bubbles and microjets affect their trajectories. These bubbles are generated by the microjet that we test and other microjets within its vicinity. In order to verify that the characterization of the magnetic dipole moment using the *U-turn* technique is indeed valid, we also calculate the magnetic dipole moment using the *rotating field* technique [19].

2) *Rotating Field Technique*: Under the influence of rotating magnetic fields, a microjet undergoes circular trajectories [20]. Increasing the frequency of the rotating fields and observing the frequency, i.e., boundary frequency, after which, the microjet no longer follows the fields allows us to calculate the magnetic dipole moment using [19]

$$|\mathbf{m}||\mathbf{B}(\mathbf{P})| + \alpha\omega_b = 0 \quad (9)$$

where ω_b is the boundary frequency of the microjet. Fig. 4 shows the motion of a microjet under the influence of rotating magnetic fields. We gradually increase the frequency of the rotating fields to determine the boundary frequency of the microjets. Rotating magnetic fields are generated using our magnetic system by simultaneously applying sinusoidal current inputs to electromagnets B and C (see Fig. 1). In the representative experiment, shown in Fig. 4, we observe that the boundary frequency of the microjet is 17 rad/s at the magnetic field of 2 mT. We repeat this experiment ten times and the average boundary frequency is calculated to be 25 ± 7 rad/s. Using (9), the magnetic dipole moment is 1.5×10^{-13} A.m² at a magnetic field of 2 mT.

Unlike the *U-turn* technique, the *rotating field* technique is time consuming. Each rotating field trial takes approximately 3 min, whereas *U-turn* trails are almost instantaneous. The mi-

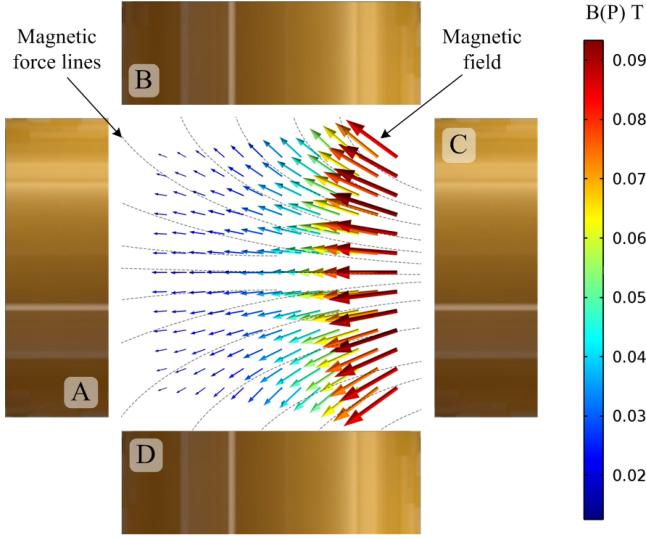


Fig. 5. FE simulation of the magnetic fields generated using electromagnet (C). Schematic representation of the magnetic force field lines is represented using the black dashed lines. The FE model is created using Comsol Multiphysics (COMSOL, Inc., Burlington, VT, USA) and is verified by measuring the magnetic fields using a calibrated three-axis Hall magnetometer (Sentron AG, Digital Teslameter 3MS1-A2D3-2-2T, Switzerland). The magnetic fields and force fields have the same direction *only* within the workspace of our system [25]. This observation allows us to control the direction of the magnetic fields by controlling the magnetic force.

crojet undergoes a *U-turn* once the magnetic field is reversed, while increasing the frequency of the rotating fields and observing the boundary frequency takes more time. This results in a change in the dynamic viscosity of the hydrogen peroxide solution due to the chemical reaction between the microjet and the solution within its vicinity. Therefore, we attribute the difference between the characterized average magnetic dipole moments to the change in the dynamic viscosity of hydrogen peroxide during each technique. Nevertheless, there is a correlation between the characterized values of the magnetic dipole moment, but these techniques have to be adapted to account for the time-varying viscosity, the bubbles-microjets interactions and microjet-microjet interactions. We use the average magnetic dipole moment ($1.4 \times 10^{-13} \text{ A}\cdot\text{m}^2$) in the realization of a nominal magnetic force-current map of our magnetic system. This map is used in the implementation of a closed-loop control system that compensates for the deviation between the actual and characterized magnetic dipole moment.

III. CONTROL SYSTEM DESIGN

The closed-loop control of microjets is done using a magnetic system that consists of four air-core electromagnets (see Fig. 2). The magnetic field lines and the magnetic force lines have the same direction *only* within the workspace of our magnetic system [25], as shown in Fig. 5. Therefore, controlling the magnetic force allows us to control the direction of the magnetic fields toward a reference position. Although we use the magnetic force-current map in the implementation of the closed-loop control of microjets, our system does not provide enough magnetic field gradients to pull the microjets toward

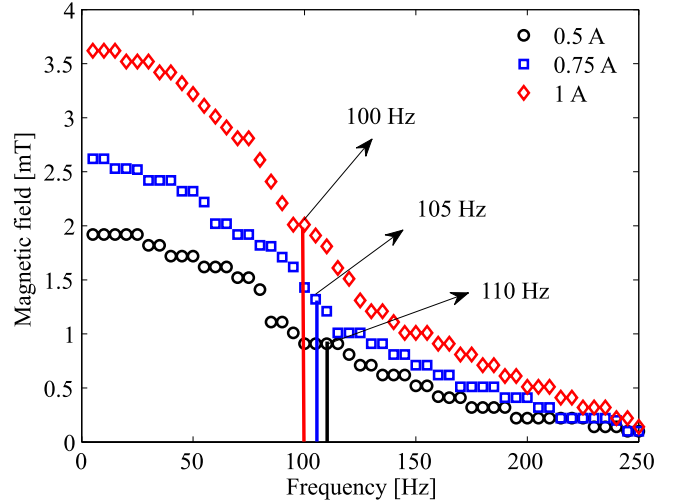


Fig. 6. Response of a single air-core electromagnet (A) to a sinusoidal current input between 5 and 250 Hz. The magnetic fields are measured at the center of the workspace of the magnetic system using a calibrated three-axis Hall magnetometer (Sentron AG, Digital Teslameter 3MS1-A2D3-2-2T, Switzerland). Our magnetic system can provide magnetic fields of 15 mT; however, current is limited to 1 A. Magnetic field magnitude is attenuated by 50% at approximately 100 Hz of the sinusoidal current input.

the reference positions. The drag force (calculated using (6) to be $1.4 \times 10^{-14} \text{ N}$) experienced by a microjet is one order of magnitude larger than the maximum magnetic force generated using our system ($8.4 \times 10^{-15} \text{ N}$ at magnetic field gradient of 60 mT/m and magnetic dipole moment of $1.4 \times 10^{-13} \text{ A}\cdot\text{m}^2$). Therefore, microjets align along the controlled field lines and move using their self-propulsion force ($\sim 7.3 \text{ pN}$) only [12].

The magnetic field can be determined by the superposition of the contribution of the i th electromagnet [4]

$$\mathbf{B}(\mathbf{P}) = \sum_{i=1}^n \mathbf{B}_i(\mathbf{P}) \quad (10)$$

where $\mathbf{B}_i(\mathbf{P})$ is the induced magnetic field by the i th electromagnet, and n is the number of electromagnets. Linearity of the magnetic field and the current allows us to rewrite (10) as follows [18]:

$$\mathbf{B}(\mathbf{P}) = \sum_{i=1}^n \tilde{\mathbf{B}}_i(\mathbf{P}) I_i = \tilde{\mathbf{B}}(\mathbf{P}) \mathbf{I}. \quad (11)$$

In (11), $\tilde{\mathbf{B}}(\mathbf{P}) \in \mathbb{R}^{3 \times n}$ is a matrix which depends on the position at which the magnetic field is evaluated, and $\mathbf{I} \in \mathbb{R}^{n \times 1}$ is a vector of the applied current. The magnetic field due to each electromagnet is related to the current input (I_i) by $\tilde{\mathbf{B}}_i(\mathbf{P})$. Substituting (11) into (3) yields the following magnetic force-current map [4], [23]:

$$\mathbf{F}(\mathbf{P}) = (\mathbf{m} \cdot \nabla) \tilde{\mathbf{B}}(\mathbf{P}) \mathbf{I} = \mathbf{\Lambda}(\mathbf{m}, \mathbf{P}) \mathbf{I} \quad (12)$$

where $\mathbf{\Lambda}(\mathbf{m}, \mathbf{P}) \in \mathbb{R}^{3 \times n}$ is the actuation matrix which maps the input current to the magnetic force [4]. We devise the following controlled magnetic force ($\mathbf{F}_c(\mathbf{P})$) to control the magnetic fields toward a fixed reference position ($\mathbf{P}_{\text{ref}} \in \mathbb{R}^{3 \times 1}$) [26]

$$\mathbf{F}_c(\mathbf{P}) = \mathbf{K}_p \mathbf{e} + \mathbf{K}_d \dot{\mathbf{e}}. \quad (13)$$

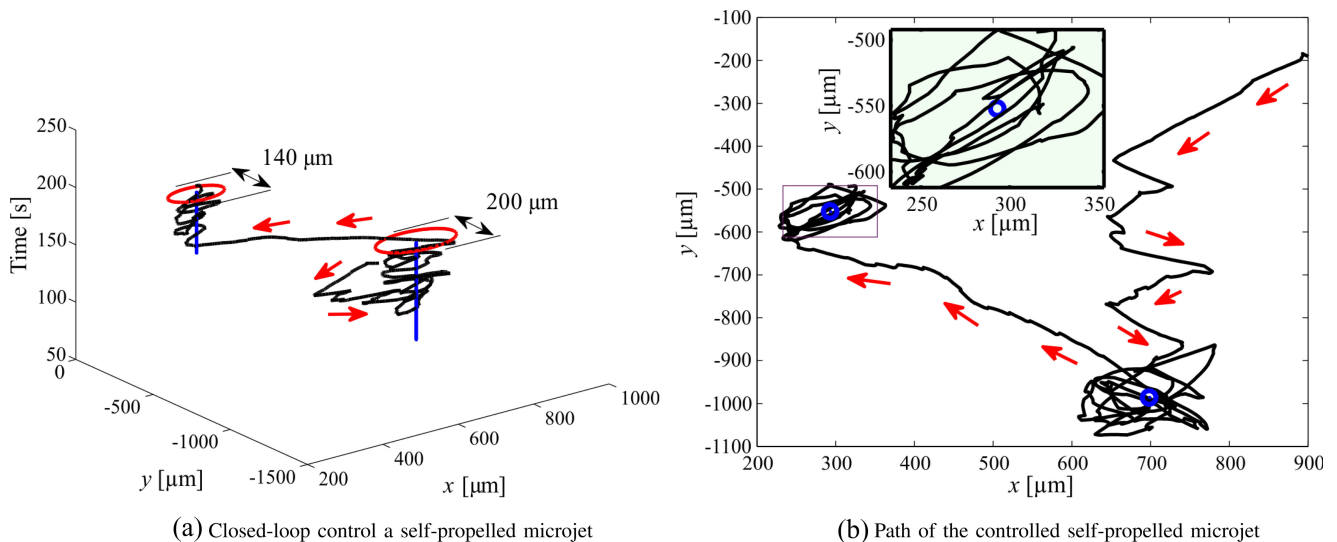


Fig. 7. Closed-loop motion control of a self-propelled microjet inside a petri dish under the influence of the controlled magnetic fields. The microjet moves toward the reference positions (small blue circles) along the magnetic field lines that are generated using the control law (13). The entries of the diagonal matrices (\mathbf{K}_p and \mathbf{K}_d) are 15 s^{-2} and 5 s^{-1} , respectively. The red arrows indicate the direction of the microjet. (a) In this representative experiment, the microjet moves at an average velocity of $90 \mu\text{m/s}$ and is positioned within the vicinity of two reference positions. (b) The closed-loop control system achieves region-of-convergence of 200 and $140 \mu\text{m}$ in diameter for the first and second reference positions, respectively. The inset shows the behavior of the controlled microjet around the reference position.

In (13), $\mathbf{K}_p \in \mathbb{R}^{3 \times 3}$ and $\mathbf{K}_d \in \mathbb{R}^{3 \times 3}$ are the controller positive-definite gain matrices. Furthermore, $\mathbf{e} \in \mathbb{R}^{3 \times 1}$ and $\dot{\mathbf{e}} \in \mathbb{R}^{3 \times 1}$ are the position and velocity tracking errors of the microjet, respectively, and are given by

$$\mathbf{e} = \mathbf{P} - \mathbf{P}_{\text{ref}} \quad \text{and} \quad \dot{\mathbf{e}} = \dot{\mathbf{P}} - \dot{\mathbf{P}}_{\text{ref}} = \dot{\mathbf{P}}. \quad (14)$$

Setting the controlled magnetic force ($\mathbf{F}_c(\mathbf{P})$) to $\mathbf{F}(\mathbf{P})$, allows us to determine the desired current at each of the electromagnets of our magnetic system. The current vector (\mathbf{I}) is calculated using the pseudoinverse of the actuation matrix (12) and is based on the characterized average magnetic dipole moment of the microjets (see Section II-B). Setting the controlled magnetic force ($\mathbf{F}_c(\mathbf{P})$) to the magnetic force in (1) yields

$$\dot{\mathbf{e}} + (\mathbf{K}_d + \alpha\eta\mathbf{I})^{-1}\mathbf{K}_p\mathbf{e} = (\mathbf{K}_d + \alpha\eta\mathbf{I})^{-1}\mathbf{F} \quad (15)$$

where \mathbf{F} is given by

$$\mathbf{F} \triangleq \mathbf{f}(\mathbf{P}, t) + \rho_f \frac{D\mathbf{u}(\mathbf{P}, t)}{Dt}. \quad (16)$$

In (15), $\mathbf{I} \in \mathbb{R}^{3 \times 3}$ is the identity matrix. The error dynamics (15) indicates that the matrix $(\mathbf{K}_d + \alpha\eta\mathbf{I})^{-1}\mathbf{K}_p$ must be positive-definite. The force (\mathbf{F}) is not zero. Therefore, the position tracking error cannot be zero, and our control system can only position the microjet within the vicinity of the reference position. The vicinity in which the microjet is positioned using control law (13) is denoted as the region-of-convergence (ROC). The ROC is further used as a measure for the positioning accuracy of the microjets. The size of the ROC is influenced by the propulsion force of the microjet, the flow rate of the hydrogen peroxide, and the controller gains based on (15). The magnetic dipole moment of the microjets and the frequency response of the electromagnets also influence the size of the ROC as the control system makes multiple magnetic field re-

TABLE I
EXPERIMENTAL PARAMETERS, CONTROLLER GAINS, AND CHARACTERIZED MAGNETIC PROPERTIES OF OUR MAGNETIC SYSTEM AND SELF-PROPELLED MICROJET. MAXIMUM MAGNETIC FIELD ($\mathbf{B}(\mathbf{P})$) AND GRADIENT ARE PROVIDED. THE CONTROLLER GAINS ARE SELECTED SUCH THAT THE MATRICES (\mathbf{K}_p AND \mathbf{K}_d) ARE POSITIVE-DEFINITE. THE ENTRIES OF THE DIAGONAL MATRICES (\mathbf{K}_p AND \mathbf{K}_d) ARE DENOTED WITH $k_{p1:p2}$, AND $k_{d1;d2}$, RESPECTIVELY. I_i AND n REPRESENT THE CURRENT AND THE NUMBER OF ELECTROMAGNETS, RESPECTIVELY

Parameter	Value	Parameter	Value
$\max I_i$ [A]	1.0	n	4
$\nabla \mathbf{B}(\mathbf{P}) $ [$\text{T}\cdot\text{m}^{-1}$]	0.06	$ \mathbf{B}(\mathbf{P}) $ [mT]	15
D [μm]	90 ± 53	η [mPa.s]	1
L [μm]	50	d [μm]	5
$k_{p1;p2}$ [s^{-2}]	15	$k_{d1;d2}$ [s^{-1}]	5
ω_b [rad/s]	25 ± 7	$ \mathbf{m} $ [$\text{A}\cdot\text{m}^2$]	1.4×10^{-13}

versals to keep the microjet within the vicinity of the reference position.

Frequency response of a single air-core electromagnet is determined using a sinusoidal current input of 0.5, 0.75, and 1 A (see Fig. 6). The magnetic field is attenuated by 50% at 100, 105, and 110 Hz for the 0.5, 0.75, and 1 A sinusoidal current inputs, respectively. This frequency response experiment indicates that our system has a limited frequency range. Increasing this frequency range could allow the control system to reduce the size of the ROC by achieving faster magnetic field reversals at the vicinity of a reference position. The inset in Fig. 7(b) shows the response of a controlled microjet within a reference position (blue circle).

IV. EXPERIMENTAL MOTION CONTROL RESULTS

Our experimental work is done inside a petri dish in the absence of a time-varying flow, and the transient- and steady-states

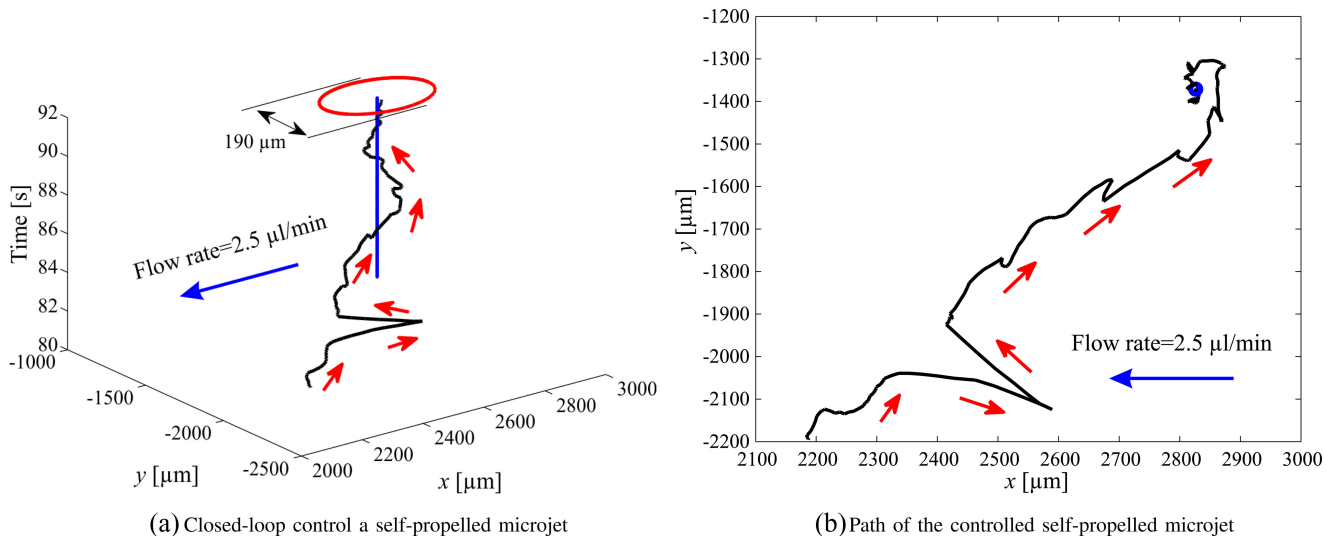


Fig. 8. Closed-loop motion control of a self-propelled microjet inside a fluidic microchannel under the influence of the controlled magnetic fields and a flow rate of $2.5 \mu\text{l}/\text{min}$ against the direction of the microjet. The microjet moves toward the reference position (small blue circle) along the magnetic field lines generated using the control law (13). The entries of the diagonal matrices (\mathbf{K}_p and \mathbf{K}_d) are 15 s^{-2} and 5 s^{-1} , respectively. The red and blue arrows indicate the direction of the microjet and the flow, respectively. (a) In this representative experiment, the microjet moves at an average velocity of $75 \mu\text{m}/\text{s}$, and it is positioned within the vicinity of a reference position. (b) The closed-loop control system achieves a ROC of $190 \mu\text{m}$ in diameter. The controlled microjet initially deviates from its path due to interaction with oxygen bubbles then aligns itself again along the field lines using the magnetic torque and the flowing streams of the hydrogen peroxide solution (blue arrow).

of the closed-loop control characteristics are determined. The effect of the time-varying flow rates on these characteristics is analyzed experimentally by controlling the microjets inside a fluidic microchannel. Furthermore, motion control characteristics are analyzed when the microjet is controlled against and along controlled time-varying flows of the hydrogen peroxide solution.

A. Experimental Setup

The experimental system consists of an array of air-core electromagnets, fluidic microchannel, and a syringe pump (see Figs. 1 and 2). The array of electromagnet surrounds a microchannel holder and the microchannel. The inlet of the microchannel is connected to the syringe pump (CMA 402 Syringe Pump, CMA Microdialysis, Kista, Sweden) using tubes with inner diameter of 0.12 mm . The width and depth of the microchannel are 500 and $300 \mu\text{m}$, respectively. The syringe pump is used to provide hydrogen peroxide solution inside the microchannel at flow rates ranging from 0 to $7.5 \mu\text{l}/\text{min}$ [16]. This range is devised based on the flow rates of blood of the vein (diameter of 5 mm and flow rate of $3\text{--}5 \text{ mm}/\text{s}$), venule (diameter of $20 \mu\text{m}$ and flow rate less than $3 \text{ mm}/\text{s}$), and capillary (diameter of $8 \mu\text{m}$ and flow rate of $1 \text{ mm}/\text{s}$) in humans [2]. The motion of the microjet is observed and tracked using a microscopic system and our feature tracking software, respectively. We analyze the performance of our closed-loop control system in the absence and presence of controlled time-varying fluid flows. The first set of experiments is done inside a petri dish, whereas the other experiments are done inside a fluidic microchannel and using the syringe pump. Experimental parameters and controller gains are included in Table I.

B. Motion Control Inside a Petri Dish

In order to analyze the control characteristics in the absence of fluid flow, we control the motion of the microjets in a petri dish using control law (13). Fig. 7 shows a representative closed-loop motion control result. Two reference positions are given to the control system, and we observe that the microjet follows the reference positions at an average velocity of $90 \mu\text{m}/\text{s}$. Furthermore, our control system achieves ROC of 200 and $140 \mu\text{m}$ for the first and second reference positions, respectively, as shown in Fig. 7(a). The inset in Fig. 7 shows the closed-loop behavior of the microjet within the vicinity of the second reference position. This closed-loop motion control trial is repeated five times, the average velocity and average ROC of the controlled microjets are calculated to be 119 and $390 \mu\text{m}$, respectively.

C. Motion Control Inside a Microchannel Against the Flow

Inside the fluidic microchannel, flow of the hydrogen peroxide solution is controlled and four flow rates are induced, i.e., 0 , 2.5 , 5 , and $7.5 \mu\text{l}/\text{min}$. Control law (13) is implemented to control the motion of the microjets at each of the mentioned flow rates using similar controller gains. In this experiment, we induce flow rates against the direction of motion of our microjets. We repeat this closed-loop experiment five times for each flow rate. Fig. 8 provides a representative experimental result at flow rate of $2.5 \mu\text{l}/\text{min}$ inside the fluidic microchannel. The microjet moves at an average velocity of $75 \mu\text{m}/\text{s}$ and is positioned within an ROC of $190 \mu\text{m}$. The average velocity and average ROC are $90 \mu\text{m}/\text{s}$ and $600 \mu\text{m}$, respectively, at flow rate of $2.5 \mu\text{l}/\text{min}$. At flow rates of 5 and $7.5 \mu\text{l}/\text{min}$, the average velocities and average ROC are calculated to be $80 \mu\text{m}/\text{s}$ and $1100 \mu\text{m}$, and $40 \mu\text{m}/\text{s}$ and $900 \mu\text{m}$, respectively.

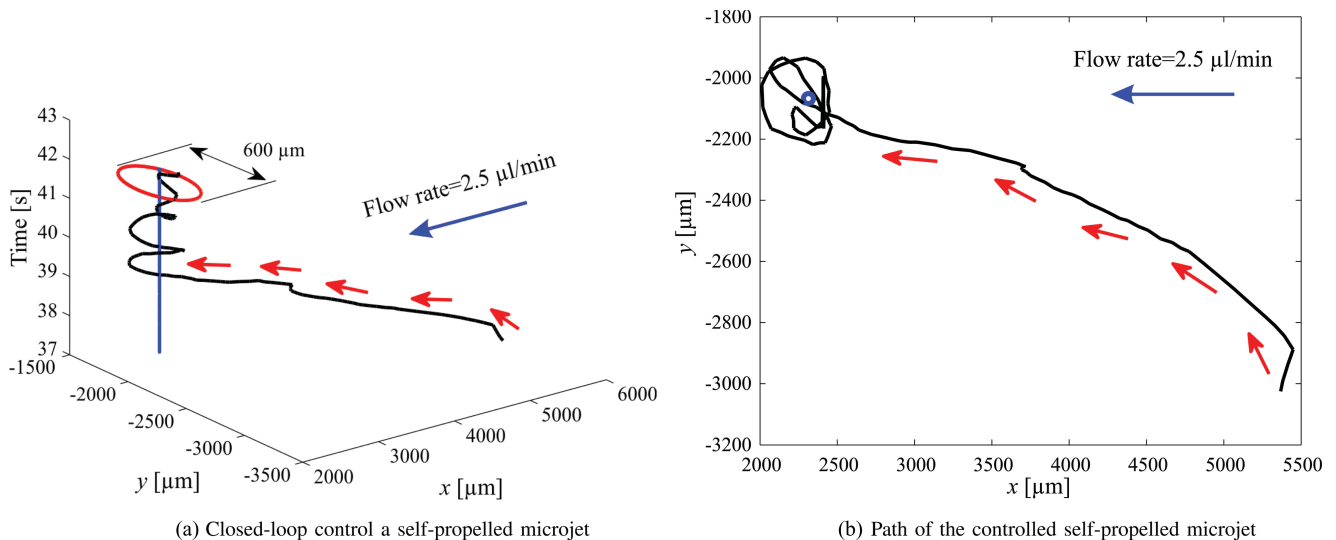


Fig. 9. Closed-loop motion control of a self-propelled microjet inside a fluidic microchannel under the influence of the controlled magnetic fields and a flow rate of $2.5 \mu\text{l}/\text{min}$ along the direction of the microjet. The microjet moves toward the reference position (small blue circle) along the magnetic field lines generated using the control law (13). The entries of the diagonal matrices (\mathbf{K}_p and \mathbf{K}_d) are 15 s^{-2} and 5 s^{-1} , respectively. The red and blue arrows indicate the direction of the microjet and the flow, respectively. (a) In this representative experiment, the microjet moves at a velocity of $155 \mu\text{m}/\text{s}$ and is positioned within the vicinity of a reference position. (b) Closed-loop control system achieves a ROC of $600 \mu\text{m}$ in diameter.

D. Motion Control Inside a Microchannel Along the Flow

Motion control of self-propelled microjets is done inside the fluidic microchannel at flow rates of 0, 2.5, 5, and $7.5 \mu\text{l}/\text{min}$. In this experiment, the flow is induced along the direction of the microjet. Control law (13) is implemented to control the motion of the microjets at each of the mentioned flow rates using similar controller gains. We repeat this closed-loop experiment five times at each flow rate. Fig. 9 provides a representative experimental result at flow rate of $2.5 \mu\text{l}/\text{min}$ inside the fluidic microchannel. In this experiment, the microjet moves at an average velocity of $155 \mu\text{m}/\text{s}$ and is positioned within a ROC of $600 \mu\text{m}$. The average velocity and average ROC are $120 \mu\text{m}/\text{s}$ and $600 \mu\text{m}$, respectively, at flow rate of $2.5 \mu\text{l}/\text{min}$. At flow rates of 5 and $7.5 \mu\text{l}/\text{min}$, the average velocities and average ROC are calculated to be $140 \mu\text{m}/\text{s}$ and $900 \mu\text{m}$, as well as $170 \mu\text{m}/\text{s}$ and $1100 \mu\text{m}$, respectively.

Fig. 10 shows the calculated average velocities and average ROC of the microjets at each flow rate, as well as for flows against and along the direction of the microjets. We observe that the velocity of the microjet increases when the flow is applied along its direction of motion. However, the positioning accuracy of the control against the flow is approximately 17% higher than the positioning accuracy of the control along the flow. We attribute the difference in the positioning accuracy to the overshoot of the microjet that occurs when we increase the flow rate along the direction of motion. By comparing Fig. 8(b) and Fig. 9(b), it is seen that the microjets exhibit larger overshoot when the flow is induced along the direction of motion. Therefore, our microjets move along the flow direction at higher velocity but are positioned within larger ROC, as opposed to microjets that move against the flow direction.

Inside the fluidic microchannels, we observe that oxygen bubbles are trapped and their diffusion rate is lower than the diffusion rate inside a petri dish (see Fig. 7). Therefore, microjets inside microchannels are not only influenced by the time-varying flow rates of the hydrogen peroxide solution but are more affected by the interaction forces with the oxygen bubbles as well.

V. CONCLUSION AND FUTURE WORK

Point-to-point motion control of self-propelled microjets is accomplished inside a fluidic microchannel with time-varying flow rates ranging from 0 to $7.5 \mu\text{l}/\text{min}$. These rates are applied against and along the direction of the microjets. The transient and steady-state characteristics, in terms of average velocity and average ROC, are evaluated in each case. At the zero flow rate, our closed-loop control system positions the microjet at an average velocity of $119 \mu\text{m}/\text{s}$ and within the vicinity of a reference position with an average ROC of $390 \mu\text{m}$. Increasing the flow rate against the direction of the microjet by $2.5 \mu\text{l}/\text{min}$ decreases and increases the average velocity and average ROC by approximately 30% and 23%, respectively. Furthermore, increasing the flow rate along the direction of the microjet by $2.5 \mu\text{l}/\text{min}$ increases and decreases the average velocity and average ROC by approximately 10% and 28%, respectively. These motion control results show that the microjets can overcome the drag forces and torques due to a controlled flow inside a fluidic microchannel.

As part of future work, the microjets will be controlled in the 3-D space inside fluidic microchannels with time-varying flow rates. In addition, we will implement an adaptive motion control system to compensate for the induced time-varying flow rates inside the microchannels and to improve the positioning accuracy of our control system. Furthermore, a characterization

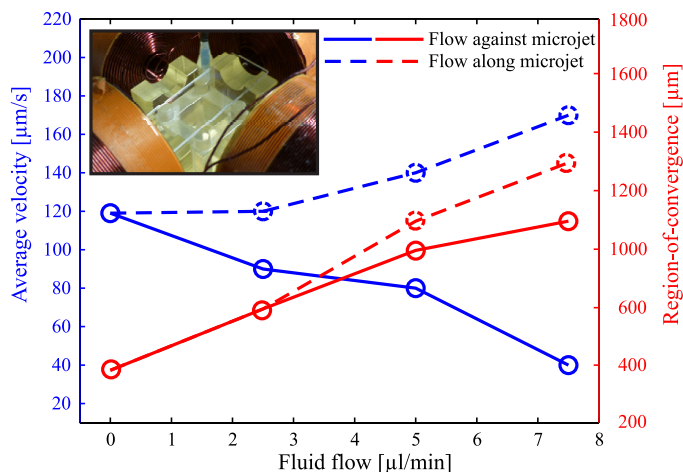


Fig. 10. Average velocity and average ROC of the controlled microjets against and along flow rates. The averages are calculated from five motion control trials in each case. These control trials are done using control law (13). The averages are calculated for four flow rates of the hydrogen peroxide solution, i.e., 0 $\mu\text{l}/\text{min}$, 2.5 $\mu\text{l}/\text{min}$, 5 $\mu\text{l}/\text{min}$, and 7.5 $\mu\text{l}/\text{min}$. (Blue) Average velocity of the controlled microjets versus four flow rates of the solution. The average velocity of the microjet decreases and increases when microjets move against and along the controlled flow of the solution, respectively. (Red) Average ROC of the controlled microjets versus Four flow rates of the solution. The ROC increases as we increase the flow rate of the solution inside the microchannel. Maximum errors in the velocity and ROC are 80 $\mu\text{m}/\text{s}$ and 800 μm , respectively.

technique for the magnetic dipole moment will be studied to account for the time-varying dynamic viscosity and the bubble–microjet interactions. Moreover, our magnetic system will be integrated with an ultrasound imaging modality to provide the motion control system with the position of the microjets in situations where visual feedback cannot be provided via a camera system.

ACKNOWLEDGMENT

The authors would like to thank the anonymous reviewers for their valuable feedback and suggestions that improved this paper. They would also like to thank M. P. Pichel for his technical assistance in conducting the experiments.

REFERENCES

- [1] R. Sinha, G. J. Kim, S. Nie, and D. M. Shin, “Nanotechnology in cancer therapeutics: Bioconjugated nanoparticles for drug delivery,” *Molecul. Cancer Therapeut.*, vol. 5, no. 8, pp. 1909–1917, Aug. 2006.
- [2] B. J. Nelson, I. K. Kaliakatsos, and J. J. Abbott, “Microrobots for minimally invasive medicine,” *Annu. Rev. Biomed. Eng.*, vol. 12, pp. 55–85, Apr. 2010.
- [3] S. Martel, O. Felfoul, J.-B. Mathieu, A. Chanu, S. Tamaz, M. Mohammadi, M. Mankiewicz, and N. Tabatabaei, “MRI-based medical nanorobotic platform for the control of magnetic nanoparticles and flagellated bacteria for target interventions in human capillaries,” *Int. J. Robot. Res.*, vol. 28, no. 9, pp. 1169–1182, Sep. 2009.
- [4] M. P. Kummer, J. J. Abbott, B. E. Kratochvil, R. Borer, A. Sengul, and B. J. Nelson, “OctoMag: An electromagnetic system for 5-DOF wireless micromanipulation,” *IEEE Trans. Robot.*, vol. 26, no. 6, pp. 1006–1017, Dec. 2010.
- [5] J. J. Abbott, Z. Nagy, F. Beyeler, and B. J. Nelson, “Robotics in the small—Part I: Microbotics,” *IEEE Robot. Autom. Mag.*, vol. 14, no. 2, pp. 92–103, Jun. 2007.
- [6] L. Dong and B. J. Nelson, “Tutorial—Robotics in the small—Part II: Nanorobotics,” *IEEE Robot. Autom. Mag.*, vol. 14, no. 3, pp. 111–121, Sep. 2007.
- [7] K. B. Yesin, K. Vollmers, and B. J. Nelson, “Modeling and control of untethered biomicrobots in a fluidic environment using electromagnetic fields,” *Int. J. Robot. Res.*, vol. 25, no. 4–5, pp. 527–536, May 2006.
- [8] S. Floyd, C. Pawashe, and M. Sitti, “Two-dimensional contact and non-contact micromanipulation in liquid using an untethered mobile magnetic microbot,” *IEEE Trans. Robot.*, vol. 25, no. 6, pp. 1332–1342, Dec. 2009.
- [9] C. Pawashe, S. Floyd, E. Diller, and M. Sitti, “Two-dimensional autonomous microparticle manipulation strategies for magnetic microrobots in fluidic environments,” *IEEE Trans. Robot.*, vol. 28, no. 2, pp. 467–477, Apr. 2012.
- [10] B. E. Kratochvil, M. P. Kummer, S. Erni, R. Borer, D. R. Frutiger, S. Schürle, and B. J. Nelson, “MiniMag: A hemispherical electromagnetic system for 5-DOF wireless micromanipulation,” presented at the 12th Int. Symp. Exp. Robotics, New Delhi, India, Dec. 2010.
- [11] K. E. Peyer, L. Zhang, and B. J. Nelson, “Bio-inspired magnetic swimming microrobots for biomedical applications,” *Nanoscale*, vol. 5, pp. 1259–1272, Nov. 2012.
- [12] S. Sanchez, A. A. Solovev, S. M. Harazim, and O. G. Schmidt, “Micro-robots swimming in the flowing streams of microfluidic channels,” *J. Amer. Chem. Soc.*, vol. 133, no. 4, pp. 701–703, Dec. 2010.
- [13] Y. F. Mei, G. Huang, A. A. Solovev, E. B. Urena, I. Monch, F. Ding, T. Reindl, R. K. Y. Fu, P. K. Chu, and O. G. Schmidt, “Versatile approach for integrative and functionalized tubes by strain engineering of nanomembranes on polymers,” *Adv. Mater.*, vol. 20, no. 21, pp. 4085–4090, Nov. 2008.
- [14] S. Sanchez, A. A. Solovev, S. Schulze, and O. G. Schmidt, “Controlled manipulation of multiple cells using catalytic microbots,” *Chem. Commun.*, vol. 47, pp. 698–700, Nov. 2010.
- [15] A. A. Solovev, S. Sanchez, M. Pumera, Y. F. Mei, and O. G. Schmidt, “Magnetic control of tubular catalytic microbots for the transport, assembly, and delivery of micro-objects,” *Adv. Funct. Mater.*, vol. 20, no. 15, pp. 2430–2435, Aug. 2010.
- [16] A. Nacev, C. Beni, O. Bruno, and B. Shapiro, “Magnetic nanoparticle transport within flowing blood and into surrounding tissue,” *Nanomed.*, vol. 5, no. 9, pp. 1459–1466, Nov. 2010.
- [17] A. S. Bahaj and P. A. B. James, “Characterisation of magnetotactic bacteria using image processing techniques,” *IEEE Trans. Magn.*, vol. 29, no. 6, pp. 3358–3360, Nov. 1993.
- [18] I. S. M. Khalil, M. P. Pichel, L. Zondervan, L. Abelmann, and S. Misra, “Characterization and control of biological microrobots,” in *Proc. 13th Int. Symp. Exp. Robot.-Springer Tracts Adv. Robot.*, Springer Tracts in Advanced Robotics, 2013, vol. 88, pp. 617–631.
- [19] B. Steinberger, N. Petersen, H. Petermann, and D. G. Wiess, “Movement of magnetic bacteria in time-varying magnetic fields,” *J. Fluid Mech.*, vol. 273, pp. 189–211, May 1994.
- [20] A. A. Solovev, Y. F. Mei, E. B. Urena, G. Huang, and O. G. Schmidt, “Catalytic microtubular jet engines self-propelled by accumulated gas bubbles,” *Small*, vol. 5, no. 14, pp. 1688–1692, Jul. 2009.
- [21] T. H. Boyer, “The force on a magnetic dipole,” *Amer. J. Phys.*, vol. 56, no. 8, pp. 688–692, Aug. 1988.
- [22] S. S. Shevkoplyas, A. C. Siegel, R. M. Westervelt, M. G. Prentiss, and G. M. Whitesides, “The force acting on a superparamagnetic bead due to an applied magnetic field,” *Lab Chip*, vol. 7, no. 6, pp. 1294–1302, Jul. 2007.
- [23] I. S. M. Khalil, M. P. Pichel, L. Abelmann, and S. Misra, “Closed-loop control of magnetotactic bacteria,” *Int. J. Robot. Res.*, vol. 32, no. 6, pp. 637–649, May 2013.
- [24] Y. R. Chemla, H. L. Grossman, T. S. Lee, J. Clarke, M. Adamkiewicz, and B. B. Buchanan, “A new study of bacterial motion: Superconducting quantum interference device microscopy of magnetotactic bacteria,” *Biophys. J.*, vol. 76, pp. 3323–3330, Jun. 1999.
- [25] J. J. Abbott, O. Ergeneman, M. P. Kummer, A. M. Hirt, and B. J. Nelson, “Modeling magnetic torque and force for controlled manipulation of soft-magnetic bodies,” *IEEE Trans. Robot. Autom.*, vol. 23, no. 6, pp. 1247–1252, Dec. 2007.
- [26] I. S. M. Khalil, V. Magdanz, S. Sanchez, O. G. Schmidt, L. Abelmann, and S. Misra, “Magnetic control of potential microrobotic drug delivery systems: Nanoparticles, magnetotactic bacteria, and self-propelled microjets,” in *Proc. Int. Conf. IEEE Eng. Med. Biol. Soc.*, Osaka, Japan, Jul. 2013, pp. 5299–5302.



Islam S. M. Khalil (S'07–M'11) received the Master's and Ph.D. degrees in mechatronics engineering from Sabanci University, Istanbul, Turkey.

He is currently an Assistant Professor with the German University, New Cairo, Egypt, and affiliated with the Production Engineering Department with Helwan University, Helwan, Egypt. For two years he was a Postdoctoral Research Associate with the Robotics and Mechatronics Research Group and MIRA–Institute for Biomedical Technology and Technical Medicine, University of Twente, Enschede,

The Netherlands. His research interests include modeling and design of motion control systems, mechatronic system design, and untethered magnetic micro/nanorobotics with applications to micro/nanomanipulation, microassembly, and targeted drug delivery.



Veronika Magdanz received the Diploma degree in biotechnology from the University of Technology, Braunschweig, Germany, in 2010. She is currently working toward the Ph.D. degree with the Institute for Integrative Nanosciences, IFW Dresden, Dresden, Germany.

In her final thesis, she developed a microbioreactor for the continuous cultivation of *S. cerevisiae*. Her research interest includes the development of artificial and biological hybrid microrobots.

Mrs. Magdanz received a DAAD/ISAP scholarship to attend the Chemical Engineering program, University of Waterloo, Waterloo, Canada, during her studies.



Samuel Sanchez received the Ph.D. degree in chemistry from the Autonomous University of Barcelona, Barcelona, Spain, in June 2008, developing electrochemical nanobiosensors.

In February 2009, he accepted a tenure-track position to work on catalytic nanomotors with the International Research Center for Materials Nanoarchitectonics, National Institute for Materials Science, Ibaraki, Japan. Since May 2010, he has been leading the “Biochemical Nanomembranes” Group with the Institute for Integrative Nanosciences at the Leibniz

Institute (IFW), Dresden, Germany. He is currently with the Max Planck Institute for Intelligent Systems, Stuttgart, Germany. His research interests include nanorobotics, biophysics, and integrated biosensors.

Dr. Sanchez received the IIN-IFW Award in 2011, the Guinness World Record® for the smallest man-made jet engine, and the ERC-Starting Grant 2012 “Lab-in-a-tube and Nanorobotic Biosensors (LT-NRBS).”



Oliver G. Schmidt is a Director at the IFW Dresden, Germany, and holds a full Professorship for Material Systems for Nanoelectronics at the Chemnitz University of Technology, Germany. His scientific activities bridge across interdisciplinary research fields, ranging from nanophotonics and energy storage to nanorobotics and microbiology.

Prof. Schmidt has received several awards: the Otto-Hahn Medal from the Max-Planck-Society in 2000, the Philip-Morris Research Award in 2002 and the Carus-Medal from the German Academy of Natural Scientists Leopoldina in 2005. In 2010, he was awarded the Guinness World Record for the smallest man-made jet engine. He has published more than 400 articles, given more than 200 invited talks and has an H-index of 52.



Sarthak Misra (S'05–M'10) received the Master's and Ph.D. degrees in mechanical engineering from McGill University, Montreal, QC, Canada, and the Johns Hopkins University, Baltimore, MD, USA, respectively.

He is currently an Associate Professor (Robotics and Mechatronics), affiliated with MIRA–Institute for Biomedical Technology and Technical Medicine, University of Twente, Enschede, The Netherlands. Prior to commencing his studies at Johns Hopkins, he worked for three years as a Dynamics and Controls Analyst on the International Space Station Program. His research interests include biomechanics and surgical robotics.

Dr. Misra received the 2010 Netherlands Organization for Scientific Research VENI award. He is an Associate Editor of the IEEE Robotics and Automation Society Conference Editorial Board.